Nanoscale

Reinforcement of polymeric nanoassemblies for ultra-high drug loadings, modulation of stiffness and release kinetics, and sustained therapeutic efficacy

Journal:	*Nanoscale*
Manuscript ID	NR-COM-03-2018-001978.R1
Article Type:	Communication
Date Submitted by the Author:	15-Apr-2018

Complete List of Authors:	Ekladious, Iriny; Boston University, Dept of Biomedical Engineering Liu, Rong; Brigham and Womens Hospital Harvard Medical School, Division of Thoracic Surgery Varongchayakul, Nitinun; Boston University, Dept of Biomedical Engineering + Chemistry Mejia Cruz, Luis; University of North Carolina at Greensboro College of Arts and Sciences Todd, Daniel; University of North Carolina at Greensboro, Chemistry & Biochemistry Zhang, Heng; Boston University, Dept of Biomedical Engineering + Chemistry Oberlies, Nicholas; University of North Carolina at Greensboro, Chemistry & Biochemistry Padera, Robert; Brigham and Womens Hospital Harvard Medical School, Division of Thoracic Surgery Colson, Yolonda; Brigham and Womens Hospital Harvard Medical School, Division of Thoracic Surgery Grinstaff, Mark; Boston University, Dept of Biomedical Engineering + Chemistry

Journal Name

COMMUNICATION

Reinforcement of polymeric nanoassemblies for ultra-high drug loadings, modulation of stiffness and release kinetics, and sustained therapeutic efficacy

Received 00th January 20xx,
Accepted 00th January 20xx

DOI: 10.1039/x0xx00000x

www.rsc.org/

Iriny Ekladious,[a] Rong Liu,[b] Nitinun Varongchayakul,[a] Luis A. Mejia Cruz,[c] Daniel A. Todd,[c] Heng Zhang,[a] Nicholas H. Oberlies,[c] Robert F. Padera,[d] Yolonda L. Colson,*[b] and Mark W. Grinstaff,*[a]

The optimization of current polymeric nanoparticle therapies is restricted by low drug loadings and limited tunability of core properties. To overcome these shortcomings, a novel self-association approach is utilized to fabricate a dual-loaded poly(1,2-glycerol carbonate)-*graft*-succinic acid-paclitaxel (PGC-PTX) conjugate nanoparticle (NP) in which the physical entrapment of free paclitaxel (PTX) affords unprecedented ultra-high drug loadings > 100 wt%, modulation of mechanical stiffness, and tunable release kinetics. Despite high incorporation of free PTX (up to 50 wt%), the dual-loaded PGC-PTX nanocarriers (i.e., PGC-PTX + PTX NPs) exhibit controlled and sustained drug release over 15 days, without burst release effects. Importantly, optimization of drug/material efficiency concomitantly affords improved *in vitro* efficacy. *In vivo*, PGC-PTX + PTX NPs are safely administered at doses exceeding the median lethal dose of standard PTX, while a single high dose significantly extends survival relative to weekly PTX administrations in a murine model of peritoneal carcinomatosis.

The incorporation of chemotherapeutic agents into nanocarriers enhances the safety and efficacy of many anticancer agents, but the conundrum remains as to the optimal composition and role(s) of the carrier material.[1-7] Current research efforts primarily focus on the design of new materials and architectures with increased functionality and complexity. However, two outstanding design challenges hamper the optimization of nanocarrier mediated drug delivery: 1) maximization of drug/material efficiency (i.e., drug loading); and, 2) tunability of nanoparticle (NP) core properties. Achieving high drug/material efficiency in the development of drug carriers is imperative, as it has the potential to significantly reduce the costs of production, and additionally minimizes a patient's exposure to synthetic carrier material. Control of NP core properties enables modulation of mechanical stiffness and release kinetics, affording an opportunity to further optimize nanocarrier drug delivery system performance and expand chemotherapy dosing protocols.

Polymer-drug conjugate nanocarriers with high drug loadings (i.e., drug:carrier mass ratios) of up to 74 wt% have been previously described.[8-10] However, these reports demonstrate a robust inverse correlation between conjugated drug content and *in vitro* potency, suggesting that increasing drug/material efficiency compromises system efficacy.[10, 11] Conversely, NPs with physically entrapped agents exhibit enhanced *in vitro* efficacy with increased drug loading.[12] Nanocarriers with physically entrapped agents nonetheless suffer from low drug loadings and significant burst release (> 50% cumulative release in 24 hours).[13] Therefore, the concurrent optimization of drug/material efficiency and system efficacy remains elusive. Furthermore, release kinetics and particle stiffness are implicated in nanocarrier efficacy.[9, 11, 14-17] However, few studies focus on modulating the rate of drug liberation or mechanical stiffness in sustained-release systems, especially within a single particle design and composition. Herein, we demonstrate the mechanical reinforcement of a novel poly(1,2-glycerol carbonate)-*graft*-succinic acid-paclitaxel (PGC-PTX) conjugate nanocarrier via the addition of free paclitaxel (PTX) as a drug "binder" to achieve unprecedented ultra-high drug loadings of up to 105 wt%, and to modulate PTX release kinetics as well as nanocarrier stiffness. Importantly, increased PTX loading results in improved *in vitro* efficacy, without the need to compromise drug/material efficiency. In a murine model of peritoneal carcinomatosis, PGC-PTX NPs with additional physically entrapped PTX (i.e., PGC-PTX + PTX NPs) exhibit improved safety at high doses and significantly prolong survival even after a single intraperitoneal (IP) injection.

[a] Departments of Biomedical Engineering and Chemistry, Boston University, Boston, MA 02215, USA. Email: mgrin@bu.edu
[b] Department of Surgery, Brigham and Women's Hospital, Boston, MA 02215, USA. Email: ycolson@bwh.harvard.edu
[c] Department of Chemistry and Biochemistry, University of North Carolina at Greensboro, Greensboro, NC 27402, USA
[d] Department of Pathology, Brigham and Women's Hospital, Boston, MA 02215, USA

† Electronic Supplementary Information (ESI) available. See DOI: 10.1039/x0xx00000x

Poly(1,2-glycerol carbonate) (PGC) is chosen as the novel scaffold for PTX conjugation as it readily degrades into biocompatible building blocks: glycerol and carbon dioxide.[18-20] Additionally, each repeating unit possesses a functionalizable pendant primary hydroxy, enabling high and controlled PTX conjugation of up to 70 mol% or 74 wt%.[10] PGC is synthesized by the ring-opening copolymerization of benzyl glycidyl ether with carbon dioxide, followed by deprotection via high pressure hydrogenolysis.[18, 21] PGC is then reacted with succinic anhydride and 4-dimethylaminopyridine (DMAP) to give PGC-*graft*-succinic acid (PGC-*g*-SA).[10] PTX is subsequently conjugated to PGC via standard coupling chemistry using N,N'-dicyclohexylcarbodiimide (DCC) and DMAP to afford PGC-PTX with 34 mol% (58 wt%) PTX conjugation (Fig. 1a see ESI for synthetic details). PTX is bound at the C-2' hydroxy required for its potent cytotoxic activity.[10, 22, 23] Thus, cleavage of PTX via the hydrolysable ester linkages affords the active form. Since PGC-PTX exhibits high PTX incorporation, we hypothesized that the compatibility (i.e., potential for physicochemical interactions) of free PTX with the PGC-PTX nanocarrier will enable the physical entrapment of large quantities of free drug, resulting in ultra-high PTX loadings. Additionally, due to the increased packing density, as well as non-covalent interactions between unconjugated and conjugated PTX, we theorized that the free drug will act as a binder, enabling modulation of both the mechanical properties and release kinetics of the nanocarrier.

PGC-PTX + PTX NPs are prepared by emulsification (Fig. 1b). The core components, including PGC-PTX and free PTX, are dissolved in dichloromethane, while the surfactant, sodium dodecyl sulfate (SDS), is added to phosphate buffer. The mixture of the organic and aqueous solutions is then emulsified under an argon blanket via ultrasonication. To ensure the elimination of unassociated SDS, the colloidal suspensions are dialyzed for 24 hours in 1 L of phosphate buffer using a dialysis membrane with a 10,000 Da molecular weight cut-off. The corresponding concentration of SDS during dialysis is < 0.01 mg/mL, which is below its critical micelle concentration of 2.3 mg/mL.[24] Given the high solubility of SDS in aqueous media (> 100 mg/mL) as well as its low molecular weight (288 Da), unassociated SDS is removed during dialysis. PGC-PTX + PTX NPs are formulated with up to 50 wt% additional physically entrapped drug, demonstrating the exceptional ability of PGC-PTX nanocarriers to encapsulate free PTX. This observation is in stark contrast to the majority of drug carriers, which typically achieve < 10 wt% drug loading by encapsulation due to less optimal compatibility between drug and carrier (Table S1, ESI†). In fact, encapsulation of celecoxib, a different hydrophobic active agent with a similar partition coefficient to PTX, does not exceed 10 wt% in PGC-PTX NPs. Similarly, poly(benzyl 1,2-glycerol carbonate) (PGC-Bn) NPs exhibit a maximum PTX encapsulation of 5 wt%, highlighting the importance of physicochemical interactions between free PTX and conjugated PTX. Previous work has likewise demonstrated that increasing the compatibility between a drug and its carrier, for example, via the incorporation of aromatic groups on the polymer chain, augments drug loading by physical entrapment (up to 35 wt% free drug).[25-28]

PGC-PTX + PTX NPs exhibit sub-100 nm diameters, low dispersity, and negative zeta potentials due to the negative charge of the SDS surface coating (Fig. 2a,b and Fig. S4, ESI†). NP size does not vary with free PTX loading, confirming the ability of the free drug binder to intersperse within the polymer network (Fig. 2a). Likewise, the addition of free PTX does not impact the low dispersity of the PGC-PTX + PTX carriers, with all formulations exhibiting low polydispersity indices (PDIs) ≤ 0.1 (Fig. S4a, ESI†). PTX encapsulation efficiency (EE), or the portion of added free drug that is incorporated in the final NP suspension, exceeds 80% for all three formulations (Fig. 2c). Interestingly, EE increases with escalating PTX loading, with the average loading efficiency reaching 95% in the 50 wt% formulation. This trend indicates that increasing the density of PTX in the nanocarrier further

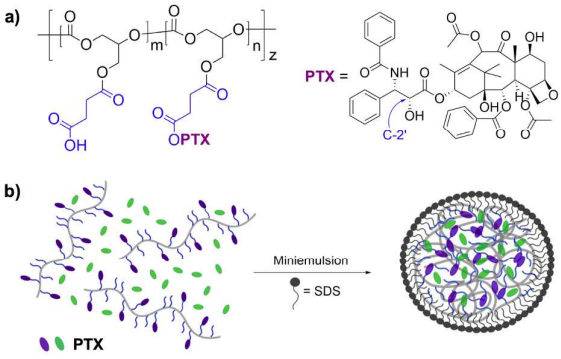

Fig. 1 Structure and formulation of PGC-PTX + PTX NPs. (a) Structure of PGC-PTX conjugate. (b) PGC-PTX + PTX NPs are formulated by emulsifying the polymer and free PTX in the presence of sodium dodecyl sulfate (SDS).

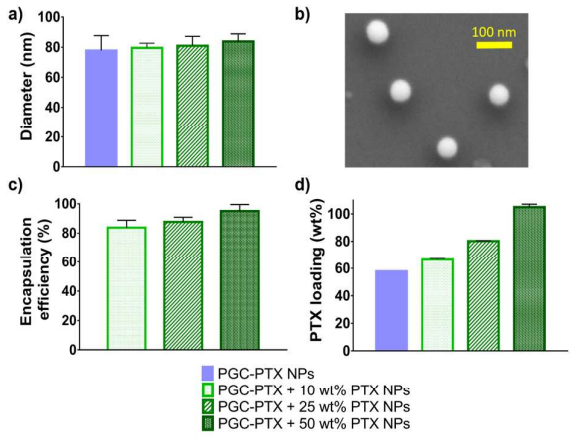

Fig. 2 Characterization of PGC-PTX + PTX NPs. (a) Dynamic light scattering size measurements of PGC-PTX NPs and PGC-PTX + PTX NPs. (b) Scanning electron micrograph of PGC-PTX + 50 wt% PTX NPs. (c) Encapsulation efficiency of free PTX. (d) Total PTX loading of each NP formulation. Data are presented as the mean ± standard deviation of 3 independently formulated NP batches per group.

promotes the incorporation of additional drug. Importantly, PGC-PTX + PTX NPs are the first demonstration of ultra-high drug loadings exceeding 100 wt%. Specifically, drug loading is defined as follows:

$$Drug\ loading\ (wt\%) = \frac{m_{drug}}{m_{carrier}} * 100\%$$

Here, m_{drug} and $m_{carrier}$ are the mass of the drug and the mass of the polymer carrier material, respectively.[25, 29, 30] Drug loading exceeds 100 wt% when the mass of the drug is greater than the mass of the carrier. Due to the high PTX incorporation in the polymer backbone as well as the enhanced ability to encapsulate large quantities of drug with high efficiency, PGC-PTX + PTX NP drug loading can be tuned from 58 wt% (PGC-PTX NPs) to 105 wt% (PGC-PTX + 50 wt% PTX NPs) (Fig. 2d). Resultant PTX concentrations are therefore as high as 20 mg/mL, compared to PTX aqueous solubility of 0.3 µg/mL.[31]

Due to the ability of PGC-PTX NPs to encapsulate free PTX at high density, we hypothesized that the free drug effectively reinforces the polymeric nanocarrier network via noncovalent interactions with conjugated PTX, rendering the free drug an effective binder for the modulation of mechanical properties on the nano-scale. To study nanocarrier mechanical properties, atomic force microscopy (AFM) was used to collect force curves, correlating cantilever tip indentation depth with force. Typical force curves display two regions with differing slopes (Fig. 3a). The initial contact regime, resulting from indentation of the particle surface, reflects the mechanical properties of the particle itself. As the tip penetrates deeper into the material, the underlying stiff substrate influences the mechanical response, altering the slope of the force curve.[32] To obtain the elastic modulus of the nanocarriers, the Hertz's model for non-adhesive elastic contact was used to correlate the loading force with indentation depth within the initial contact regime, spanning 5 – 50 pN force and up to 50 nm indentation depth. Increased free PTX loading results in significant increases in nanocarrier elastic modulus (≥ 25 wt% PTX; Fig. 3b). Interestingly, this effect is not significant at lower loadings of free PTX (≤ 10 wt%), illustrating the importance of high loading capacity. PGC-PTX NPs and PGC-PTX + PTX NPs with 10, 25, and 50 wt% free PTX exhibit elastic moduli of 27.2 ± 9.5, 39.0 ± 9.9, 55.2 ± 23.2, and 94.5 ± 20.1 kPa, respectively. These values are within the range of elastic moduli reported for polymers such as highly cross-linked polyvinylpyrrolidone (40.8 ± 1.9 kPa),[33] highly cross-linked polyacrylamide (34.8 ± 1.5 kPa),[33] high density poly(N-isopropylacrylamide) (123 ± 9 kPa),[34] and agar (40-90 kPa).[35] The ability of PTX to mechanically reinforce the nanocarrier polymer network is attributed to increased packing density as well as interactions of the drug with the polymer scaffold. Similarly, crystals exhibit high stiffness due to high packing density and molecular order. To evaluate the stiffness of highly ordered PTX in the absence of a polymer network, PTX crystals were formed by emulsifying a solution of the free drug in an aqueous solution of SDS (Fig. S5, ESI†). PTX crystals exhibit an elastic modulus of 796 ± 565 MPa, four orders of magnitude greater than the polymeric nanocarrier formulations. Nonetheless, despite their high PTX loading, the PGC-PTX + PTX nanocarriers do not exhibit crystallinity as demonstrated by differential scanning calorimetry and x-ray powder diffraction analysis, confirming the random distribution of PTX within the entangled polymer network (Fig. S6 and Fig. S7, ESI†). This result is in agreement with previous reports demonstrating the amorphous configuration of active agents, including PTX and docetaxel, in polymeric carriers.[12, 36, 37]

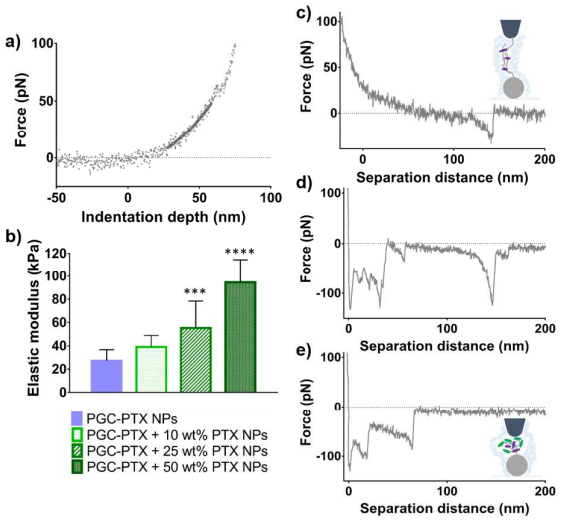

Fig. 3 Nanomechanical characterization of PGC-PTX + PTX NPs. (a) Representative force-indentation curve of a nanoparticle. The solid line shows the region used for fitting using the Hertz's model. (b) Elastic modulus of NP formulations (***p < 0.001, ****p < 0.0001; compared to PGC-PTX NPs). Data are presented as mean ± standard deviation. Example force retraction curves showing (c) single extension peak, (d) saw-tooth pattern, and (e) irregular force plateau. Insets illustrate the proposed mechanism of polymer chain pulling.

Analysis of AFM retraction curves reveals long-range adhesive interactions between polymer chains in the nanocarrier matrix. All PGC-PTX + PTX NPs exhibit rupture lengths on the order of 100 nm (Fig. S8, ESI†), while previous size exclusion chromatography measurements illustrate that PGC-PTX exhibits an average molecular weight of 9,393 Da, corresponding to an 18-mer with an extended chain-length of approximately 16 nm.[10] This result suggests that many interacting chains are concurrently pulled by the AFM tip. Individual analysis of force retraction curve patterns for each formulation provides additional insight on molecular interactions within the polymeric core. While 93% of the retraction curves of PGC-PTX NPs reveal single peaks resembling the pulling of a polymer chain (Fig. 3c), 7% show a saw-tooth pattern (Fig. 3d), which is typically observed in the unfolding of a structured protein or the unzipping of a polymer fiber from a substrate.[38, 39] In the case of a polymeric nanocarrier, the saw-tooth pattern is likely due to the pulling and disruption of multiple, entangled polymer chains. The force extension curves of reinforced PGC-PTX + 10 wt% PTX

NPs exhibit a greater incidence of saw-tooth patterns, at a frequency of 70%, demonstrating increased core interactions in the presence of free PTX. An additional 28% of retraction curves exhibit irregular plateau force curves (Fig. 3e), while 2% reveal single peaks. Irregular plateau force curves result from stretching of the pulled chains, which is required to overcome increased interactions in the entangled polymer network.[40, 41] At 25 wt% free PTX loading, we observe 4% single peak stretching, 50% saw-tooth pattern, and 46% irregular plateau force curves. Finally, at the highest free PTX encapsulation of 50 wt%, we rarely observe extension curves, likely due to decreased adhesion between the tip and rigid polymer matrix. Among the few extension curves observed, 6% show single peaks, 29% show a saw-tooth pattern, and 65% show irregular plateau force curves. Taken together, these results demonstrate the tunability of PGC-PTX + PTX nanocarrier mechanical properties as a function of physically entrapped PTX, which increases core stiffness and promotes polymer matrix stability via the augmentation of core interactions.

Subsequently, PTX release kinetics were evaluated by incubating the NPs in pH 7.4 phosphate buffer for 15 days at 37 °C (Fig. 4a,b). At given time-points, aliquots were collected from the release media and free PTX content was determined using liquid chromatography-mass spectrometry. PGC-PTX NPs and PGC-PTX + PTX NPs with 10, 25, and 50 wt% free PTX encapsulation exhibit 24%, 39%, 89%, and 77% cumulative PTX release within 15 days, respectively (Fig. 4b). While PGC-PTX + 50 wt% PTX NPs display accelerated drug release at early time-points (≤ 5 days) (Fig. 4a), PGC-PTX + 25 wt% PTX NPs demonstrate greater cumulative PTX release at later time-points (Fig. 4b). This result is likewise attributed to the increasing propensity of free PTX to interact with the nanocarrier matrix as overall PTX content is increased. Interestingly, scanning electron micrographs of PGC-PTX NPs and PGC-PTX + 50 wt% PTX NPs after 7 and 15 days of release show that both nanocarrier formulations exhibit a decrease in size following PTX release (Fig. S9, ESI†). However, PGC-PTX NPs maintain a stable elastic modulus throughout the 15 day release period, while PGC-PTX + 50 wt% PTX NPs exhibit significant reductions in stiffness with increased duration of release (Fig. 4c). These results are in agreement with the relatively rapid PTX release kinetics of the PGC-PTX + 50 wt% PTX NPs compared to the PGC-PTX NPs, and additionally demonstrate that liberation of PTX from the PGC-PTX + PTX nanocarrier core reduces core interactions and mechanical stiffness.

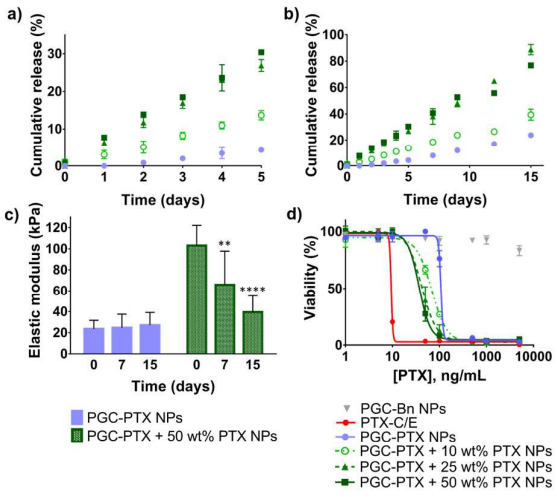

Fig. 4 PGC-PTX + PTX NP release kinetics, nanomechanical characterization following drug release, and *in vitro* cytotoxicity. PTX release kinetics of PGC-PTX NPs and PGC-PTX + PTX NPs at 37 °C in pH 7.4 phosphate buffer at (a) early time-points (≤ 5 days) and (b) over 15 days. (c) The elastic moduli of PGC-PTX NPs and PGC-PTX + 50 wt% PTX NPs were characterized before and after 7 and 15 days of release (**p < 0.01, ****p < 0.0001; compared to day 0 control). (d) MSTO-211H cells were incubated with non-drug loaded PGC-Bn NPs, PTX-C/E, or one of four NP formulations. Cell viability was evaluated after 5 days of exposure. All experiments were performed in triplicate, with data presented as the mean ± standard deviation.

PGC-PTX + PTX NPs exhibit tunable release kinetics, which are modulated by varying the free PTX content. Increasing the ratio of unconjugated:conjugated PTX via the physical entrapment of free drug affords facilitated release kinetics due to the ability of free PTX to diffuse from the polymeric matrix without the need for cleavage from the polymer backbone. However, despite the high density of free PTX, an initial burst release is not observed, with all PGC-PTX + PTX NP formulations exhibiting sustained drug release due to the compatibility between PTX and the PGC-PTX carrier. Additionally, we observe that the elastic modulus of the PGC-PTX + PTX NPs decreases with drug release time while the PGC-PTX NPs do not. Burst release kinetics of physically entrapped drug can be attenuated by increasing the compatibility between the drug and the polymer carrier, for example, via the incorporation of aromatic groups in the polymer chain.[26, 27] The release of conjugated PTX depends on both diffusion and hydrolysis of the drug from the polymer backbone. Sustained, linear release kinetics are reported for polymer-drug conjugate therapeutics.[15, 42, 43] Classically, surface erosion of a polymer depot containing an encapsulated drug affords linear release kinetics.[44] Studies are ongoing to further characterize the release mechanism of the PGC-PTX + PTX NPs, which likely involves a combination of surface and bulk erosion processes.

NP *in vitro* cytotoxicity was evaluated in MSTO-211H mesothelioma cancer cells after 5 days of exposure (Fig. 4d). Cells were treated with PGC-PTX NPs, one of the PGC-PTX + PTX NP formulations, the clinical formulation of PTX in a Cremophor EL/ethanol (1:1 v/v; C/E) excipient (PTX-C/E), or PGC-Bn NPs as a drug-free NP control. Cells treated with drug-free PGC-Bn NPs at equivalent PGC backbone concentrations to PGC-PTX NPs exhibit minimal cell death, with viabilities exceeding 80% at all concentrations. Due to the sustained release of active PTX from the PGC-PTX + PTX nanocarriers over an extended period of time, the *in vitro* potency after 5 days of exposure is reduced relative to PTX-C/E. Nonetheless, in contrast with previous reports, PGC-PTX + PTX NP potency increases with greater PTX loading, with PGC-PTX + 50 wt%

PTX NPs (105 wt% total PTX loading) exhibiting the greatest cytotoxic effect (Table S2, ESI†). These results also correlate with PGC-PTX + PTX NP release kinetics at early time-points (≤ 5 days), with accelerated drug release resulting in greater *in vitro* cell killing. Therefore, PGC-PTX + PTX NPs afford the concurrent optimization of nanocarrier drug loading and efficacy.

To evaluate the effect of rigidity on nanocarrier cellular internalization kinetics, MSTO-211H cells were incubated with either fluorescent, rhodamine-labeled PGC-PTX NPs or fluorescent, rhodamine-labeled PGC-PTX + 50 wt% PTX NPs. Nanocarrier internalization was subsequently monitored over the course of 4 hours via fluorescence activated cell sorting. Cells exhibiting greater fluorescence than 99% of the untreated, control population were considered positive for NP internalization. Our results demonstrate that the stiffer PGC-PTX + 50 wt% PTX NPs exhibit significantly increased cellular uptake at all time-points, with 96% of the cell population internalizing PGC-PTX + 50 wt% PTX NPs within 2 hours of treatment (Fig. S10, ESI†). Conversely, only 76% of cells internalize PGC-PTX NPs after 4 hours of exposure. This result is in agreement with previously published reports demonstrating greater cellular internalization of rigid nanocarriers relative to less rigid nanocarriers.[16, 17] Notably, conflicting reports regarding the effect of particle stiffness on cellular internalization warrant further and continued evaluation of tunable carriers.[45-47] NP cellular internalization, rather than cell surface adhesion, was confirmed via laser scanning confocal microscopy (Fig. S11, ESI†).

Due to the high aqueous concentrations of PTX as well as the continuous and sustained drug release afforded by the PGC-PTX + PTX nanocarriers, we hypothesized that PGC-PTX + PTX NPs can be safely administered at considerably higher PTX doses than PTX-C/E. A single dose of 140 mg/kg conjugated PTX can be safely administered in mice via PGC-PTX NPs.[10] To evaluate the safety of the analogous dual-loaded carriers, healthy mice were given a single IP injection of PGC-PTX + 25 wt% PTX NPs at a dose of 200 mg/kg PTX (140 mg/kg conjugated PTX + 60 mg/kg free PTX), and body weight was monitored over the course of two weeks post-administration. This formulation was chosen for initial evaluation as it has the median free drug loading among the NPs studied. Animals treated with PGC-PTX + 25 wt% PTX NPs exhibit an initial 10% reduction in body weight within two days after treatment (Fig. S12a, ESI†), rendering 60 mg/kg (25 wt%) free PTX the maximum dose that can be safely administered. Nonetheless, animal weight increases after day 2 and returns to starting weight by day 14. Additionally, histological evaluation of the major organs after 14 days of PGC-PTX + 25 wt% PTX NP exposure does not reveal any adverse reactions relative to untreated animal controls, confirming that the treatment is well-tolerated (Fig. S12b-g, ESI†). Therefore, a large dose of 200 mg/kg PTX can be safely administered via PGC-PTX + 25 wt% PTX NPs. In contrast, the maximum tolerated dose (MTD) of standard PTX-C/E in mice is between 13-50 mg/kg, while the median lethal dose (LD_{50}) is 128 mg/kg.[48-51]

While sustained release is desirable for maintaining high local concentrations of active drug and minimizing toxicities associated with high peak tissue concentrations, Luo *et al*. report that among three PTX nano-conjugate systems exhibiting sustained release, the system exhibiting the most rapid release is the most efficacious *in vitro* and *in vivo*.[14] Our own results as well as those of others likewise demonstrate that accelerated drug release kinetics correlate with improved *in vitro* efficacy.[9, 15] Due to the continuous and extended PTX release afforded by PGC-PTX nanocarriers, we previously demonstrated the utility of PGC-PTX NPs as a single high-dose replacement for multi-dose PTX treatment regimens in peritoneal mesothelioma.[10] A single IP injection of 140 mg/kg PTX via PGC-PTX NPs affords comparable survival to PTX administered as seven doses of weekly 20 mg/kg PTX-C/E.[10] However, we hypothesized that PGC-PTX + 25 wt% PTX NPs, which exhibit sustained PTX release over a period of 15 days compared to 70 days for PGC-PTX NPs, would significantly improve survival compared to the equivalent dose of PTX-C/E administered as a multi-dose treatment regimen. One week after IP tumor inoculation with luciferase-expressing MSTO-211H (MSTO-211H-luc) cells, mice were treated with either saline, a single dose of 200 mg/kg PTX via PGC-PTX + 25 wt% PTX NPs (140 mg/kg conjugated + 60 mg/kg unconjugated PTX), or weekly 20 mg/kg PTX-C/E for up to 10 weeks (total PTX dose equivalent). Due to the toxicity of PTX-C/E, an equivalent single high-dose control cannot be administered. Additionally, daily 20 mg/kg PTX-C/E administrations result in a 63% acute mortality rate.[10] Therefore, a total PTX-C/E dose control must be administered as a weekly multi-dose treatment regimen. The study was concluded 8 weeks after tumor inoculation when > 90% of control animals succumbed to disease. Animals treated with a single dose of PGC-PTX + 25 wt% PTX NPs exhibit significantly improved survival compared to multi-dose PTX-C/E treated animals (p=0.0105; Fig. 5). Similarly, at 4 and 6 weeks after tumor inoculation, PGC-PTX + 25 wt% PTX NP treated animals exhibit visibly reduced tumor burden relative to control groups (Fig. S13, ESI†). Therefore, a

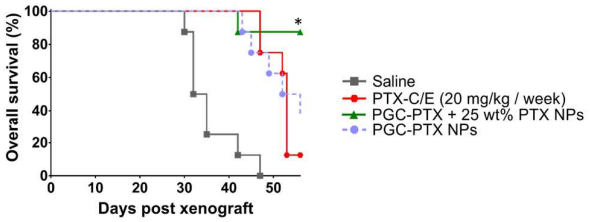

Fig. 5 *In vivo* efficacy of PGC-PTX + 25 wt% PTX NPs as a single dose in the treatment of peritoneal mesothelioma. One week after IP tumor inoculation, mice were treated with saline, a single 200 mg/kg PTX dose via PGC-PTX + 25 wt% PTX NPs (140 mg/kg conjugated PTX + 60 mg/kg free PTX), or weekly 20 mg/kg PTX-C/E for up to 10 weeks (total dose control). Overall survival was monitored for 8 weeks post-tumor inoculation (n=8 per group; *p=0.0105). Overall survival of animals treated with a single dose of 140 mg/kg PTX via PGC-PTX NPs in a separate study is shown for reference.[10]

single high dose of PGC-PTX + 25 wt% PTX NPs extends survival compared to multi-dose PTX-C/E, while polymer only PGC-PTX NPs exhibit equivalent efficacy to multi-dose PTX-C/E.[10] Given a drug release rate of approximately 6% per day (Fig. 4b), PGC-PTX + 25 wt% PTX NP *in vivo* dosing is approximated to be 12 mg/kg PTX per day, which is within the therapeutic range employed in preclinical investigation.[52-54] Accordingly, PGC-PTX + 25 wt% PTX NP treatment is not expected to cause drug resistance. Nonetheless, studies are underway to assess the sensitivity of tumor cells to PTX treatment following exposure to PGC-PTX + 25 wt% PTX NPs, as well as to quantify tumor PTX concentrations following NP treatment. These findings highlight the utility of PGC-PTX + 25 wt% PTX NPs in the treatment of peritoneal carcinomatosis, in which the implementation of long-term regional chemotherapy is challenging despite demonstrating improved outcomes.[55, 56]

Conclusions

In summary, PGC-PTX + PTX nanoassemblies are a distinctive drug delivery system which enables unprecedented ultra-high drug loadings > 100 wt% via encapsulation of free drug in a high density drug-conjugated polymer. NP formulation is robust and reproducible, producing uniform sub-100 nm particles. The self-association and physical entrapment of free PTX binder affords the modulation of PTX loading, nanocarrier stiffness, and drug release kinetics. Despite the high density of free PTX (up to 50 wt%), all PGC-PTX + PTX NP formulations exhibit sustained and controlled PTX release over 15 days, without any burst release effects. The continuous and sustained release of PTX from PGC-PTX + PTX nanocarriers affords improved *in vivo* safety at high PTX doses exceeding the LD_{50} of standard PTX-C/E. Importantly, PGC-PTX + PTX NPs enable the concurrent optimization of drug/material efficiency and system efficacy. PGC-PTX + PTX NPs with increased drug loadings exhibit improved *in vitro* efficacy. Similarly, a single high-dose of PGC-PTX + 25 wt% PTX NPs affords significantly improved survival in a murine model of peritoneal carcinomatosis compared to a multi-dose PTX-C/E treatment regimen, while polymer only PGC-PTX NPs exhibit equivalent efficacy to multi-dose PTX-C/E. Notably, these dual-loaded polymer-drug conjugate nanoassemblies present a unique platform for the modulation and optimization of nanocarrier properties. The concomitant realization of nanocarriers with previously unattainable ultra-high drug loadings, sustained release, and *in vivo* safety at high PTX doses opens new paradigms in the rational design of novel drug delivery systems and dosing protocols with transformative clinical potential.

Conflicts of interest

There are no conflicts to declare.

Acknowledgements

This work was supported in part by funding from the National Science Foundation (DGE-1247312, DMR-1507081), Brigham and Women's Hospital, and Boston University.

Notes and references

1 N. Kamaly, B. Yameen, J. Wu and O. C. Farokhzad, *Chem. Rev.*, 2016, **116**, 2602-2663.
2 S. Svenson, *Wiley Interdiscip. Rev. Nanomed. Nanobiotechnol.*, 2014, **6**, 125-135.
3 M. E. Davis, Z. G. Chen and D. M. Shin, *Nat. Rev. Drug Discov.*, 2008, **7**, 771-782.
4 R. A. Petros and J. M. DeSimone, *Nat. Rev. Drug Discov.*, 2010, **9**, 615-627.
5 D. Pan, C. T. Pham, K. N. Weilbaecher, M. H. Tomasson, S. A. Wickline and G. M. Lanza, *Wiley Interdiscip. Rev. Nanomed. Nanobiotechnol.*, 2016, **8**, 85-106.
6 Y. Min, J. M. Caster, M. J. Eblan and A. Z. Wang, *Chem. Rev.*, 2015, **115**, 11147-11190.
7 J. Yang and J. Kopecek, *J. Control. Release*, 2014, **190**, 288-303.
8 S. Zhang, J. Zou, M. Elsabahy, A. Karwa, A. Li, D. A. Moore, R. B. Dorshow and K. L. Wooley, *Chem. Sci.*, 2013, **4**, 2122-2126.
9 J. Zou, F. Zhang, S. Zhang, S. F. Pollack, M. Elsabahy, J. Fan and K. L. Wooley, *Adv. Healthcare Mater.*, 2014, **3**, 441-448.
10 I. Ekladious, R. Liu, H. Zhang, D. H. Foil, D. A. Todd, T. N. Graf, R. F. Padera, N. H. Oberlies, Y. L. Colson and M. W. Grinstaff, *Chem. Sci.*, 2017, **8**, 8443-8450.
11 M. Callari, P. L. De Souza, A. Rawal and M. H. Stenzel, *Angew. Chem. Int. Ed. Engl.*, 2017, **56**, 8441-8445.
12 E. M. Enlow, J. C. Luft, M. E. Napier and J. M. DeSimone, *Nano Lett.*, 2011, **11**, 808-813.
13 K. S. Soppimath, T. M. Aminabhavi, A. R. Kulkarni and W. E. Rudzinski, *J. Control. Release*, 2001, **70**, 1-20.
14 C. Luo, J. Sun, D. Liu, B. Sun, L. Miao, S. Musetti, J. Li, X. Han, Y. Du, L. Li, L. Huang and Z. He, *Nano Lett.*, 2016, **16**, 5401-5408.
15 R. Tong and J. Cheng, *Angew. Chem. Int. Ed. Engl.*, 2008, **47**, 4830-4834.
16 J. Sun, L. Zhang, J. Wang, Q. Feng, D. Liu, Q. Yin, D. Xu, Y. Wei, B. Ding, X. Shi and X. Jiang, *Adv. Mater.*, 2015, **27**, 1402-1407.
17 L. Zhang, Q. Feng, J. Wang, S. Zhang, B. Ding, Y. Wei, M. Dong, J. Y. Ryu, T. Y. Yoon, X. Shi, J. Sun and X. Jiang, *ACS Nano*, 2015, **9**, 9912-9921.
18 H. Zhang and M. W. Grinstaff, *J. Am. Chem. Soc.*, 2013, **135**, 6806-6809.
19 N. G. Ricapito, C. Ghobril, H. Zhang, M. W. Grinstaff and D. Putnam, *Chem. Rev.*, 2016, **116**, 2664-2704.
20 M. Calderon, M. A. Quadir, S. K. Sharma and R. Haag, *Adv. Mater.*, 2010, **22**, 190-218.
21 G. W. Coates and D. R. Moore, *Angew. Chem. Int. Ed. Engl.*, 2004, **43**, 6618-6639.
22 J. Kant, S. Huang, H. Wong, C. Fairchild, D. Vyas and V. Farina, *Bioorg. Med. Chem. Lett.*, 1993, **3**, 2471-2474.
23 H. J. Williams, G. Moyna, A. I. Scott, C. S. Swindell, L. E. Chirlian, J. M. Heerding and D. K. Williams, *J. Med. Chem.*, 1996, **39**, 1555-1559.

24 A. Cifuentes, J. L. Bernal and J. C. Diez-Masa, *Anal. Chem.*, 1997, **69**, 4271-4274.
25 X. Hu, J. Li, W. Lin, Y. Huang, X. Jing and Z. Xie, *RSC Adv.*, 2014, **4**, 38405-38411.
26 Y. Shi, M. J. van Steenbergen, E. A. Teunissen, L. Novo, S. Gradmann, M. Baldus, C. F. van Nostrum and W. E. Hennink, *Biomacromolecules*, 2013, **14**, 1826-1837.
27 A. S. Mikhail and C. Allen, *Biomacromolecules*, 2010, **11**, 1273-1280.
28 Y. Ma, X. Fan and L. Li, *Carbohydr. Polym.*, 2016, **137**, 19-29.
29 Y. Guo, X. Wang, X. Shu, Z. Shen and R. C. Sun, *J. Agric. Food Chem.*, 2012, **60**, 3900-3908.
30 S. Shen, Y. Wu, Y. Liu and D. Wu, *Int. J. Nanomedicine*, 2017, **12**, 4085-4109.
31 R. T. Liggins, W. L. Hunter and H. M. Burt, *J. Pharm. Sci.*, 1997, **86**, 1458-1463.
32 J. Domke and M. Radmacher, *Langmuir*, 1998, **14**, 3320-3325.
33 M. V. Flores-Merino, S. Chirasatitsin, C. Lopresti, G. C. Reilly, G. Battaglia and A. J. Engler, *Soft Matter*, 2010, **6**, 4466-4470.
34 X. Sui, Q. Chen, M. A. Hempenius and G. J. Vancso, *Small*, 2011, **7**, 1440-1447.
35 H. Haga, S. Sasaki, M. Morimoto, K. Kawabata, E. Ito, K. Abe and T. Sambongi, *Jpn. J. Appl. Phys.*, 1998, **37**, 3860-3863.
36 J. G. Hiremath, N. S. Khamar, S. G. Palavalli, C. G. Rudani, R. Aitha and P. Mura, *Saudi Pharm. J.*, 2013, **21**, 85-91.
37 N. Pirooznia, S. Hasannia, A. S. Lotfi and M. Ghanei, *J. Nanobiotechnology*, 2012, **10**, 20.
38 M. Rief, M. Gautel, F. Oesterhelt, J. M. Fernandez and H. E. Gaub, *Science*, 1997, **276**, 1109-1112.
39 F. Valle, G. Zuccheri, A. Bergia, L. Ayres, A. E. Rowan, R. J. Nolte and B. Samori, *Angew. Chem. Int. Ed. Engl.*, 2008, **47**, 2431-2434.
40 T. Hugel, M. Grosholz, H. Clausen-Schaumann, A. Pfau, H. Gaub and M. Seitz, *Macromolecules*, 2001, **34**, 1039-1047.
41 I. T. Li and G. C. Walker, *Proc. Natl. Acad. Sci. U. S. A.*, 2011, **108**, 16527-16532.
42 R. Iezzi, B. R. Guru, I. V. Glybina, M. K. Mishra, A. Kennedy and R. M. Kannan, *Biomaterials*, 2012, **33**, 979-988.
43 Z. Zhou, X. Ma, C. J. Murphy, E. Jin, Q. Sun, Y. Shen, E. A. Van Kirk and W. J. Murdoch, *Angew. Chem. Int. Ed. Engl.*, 2014, **53**, 10949-10955.
44 A. Gopferich and J. Tessmar, *Adv Drug Deliv Rev*, 2002, **54**, 911-931.
45 P. Guo, D. Liu, K. Subramanyam, B. Wang, J. Yang, J. Huang, D. T. Auguste and M. A. Moses, *Nat. Commun.*, 2018, **9**, 130.
46 W. Liu, X. Zhou, Z. Mao, D. Yu, B. Wang and C. Gao, *Soft Matter*, 2012, **8**, 9235-9245.
47 X. Banquy, F. Suarez, A. Argaw, J.-M. Rabanel, P. Grutter, J.-F. Bouchard, P. Hildgen and S. Giasson, *Soft Matter*, 2009, **5**, 3984-3991.
48 V. Vassileva, J. Grant, R. De Souza, C. Allen and M. Piquette-Miller, *Cancer Chemother. Pharmacol.*, 2007, **60**, 907-914.
49 A. Sharma, U. S. Sharma and R. M. Straubinger, *Cancer Lett.*, 1996, **107**, 265-272.
50 F. Danhier, N. Magotteaux, B. Ucakar, N. Lecouturier, M. Brewster and V. Preat, *Eur. J. Pharm. Biopharm.*, 2009, **73**, 230-238.
51 C. S. Kue, K. Y. Tan, M. L. Lam and H. B. Lee, *Exp. Anim.*, 2015, **64**, 129-138.
52 R. Liu, A. H. Colby, D. Gilmore, M. Schulz, J. Zeng, R. F. Padera, O. Shirihai, M. W. Grinstaff and Y. L. Colson, *Biomaterials*, 2016, **102**, 175-186.
53 V. Vassileva, E. H. Moriyama, R. De Souza, J. Grant, C. J. Allen, B. C. Wilson and M. Piquette-Miller, *Br. J. Cancer*, 2008, **99**, 2037-2043.
54 T. Kubota, S. W. Matsuzaki, Y. Hoshiya, M. Watanabe, M. Kitajima, F. Asanuma, Y. Yamada and J. I. Koh, *J. Surg. Oncol.*, 1997, **64**, 115-121.
55 P. H. Sugarbaker and D. Chang, *Eur. J. Surg. Oncol.*, 2017, **43**, 1228-1235.
56 D. K. Armstrong, B. Bundy, L. Wenzel, H. Q. Huang, R. Baergen, S. Lele, L. J. Copeland, J. L. Walker and R. A. Burger, *N. Engl. J. Med.*, 2006, **354**, 34-43.

The ORCID IDs

Iriny Ekladious	0000-0003-1192-1414
Rong Liu	0000-0001-5876-1986
Nitinun Varongchayakul	0000-0002-7612-4478
Luis A. Mejia Cruz	0000-0003-2924-209X
Daniel A. Todd	0000-0003-2199-1029
Heng Zhang	0000-0002-7475-4185
Nicholas H. Oberlies	0000-0002-0354-8464
Robert F. Padera	0000-0002-4571-5494
Yolonda L. Colson	0000-0002-8229-5636
Mark W. Grinstaff	0000-0002-5453-3668

Table of Contents Entry

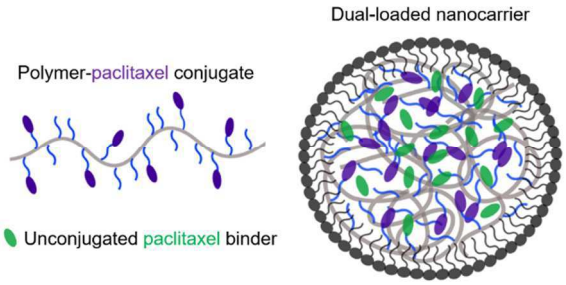

A novel, dual-loaded nanocarrier affords unprecedented ultra-high drug loadings, modulation of mechanical stiffness and release kinetics, and sustained therapeutic efficacy.